Mineralium Deposita (2007) 42: 51–64
DOI 10.1007/s00126-005-0012-z

ARTICLE

Daniela A. Vallini · David I. Groves
Neal J. McNaughton · Ian R. Fletcher

Uraniferous diagenetic xenotime in northern Australia and its relationship to unconformity-associated uranium mineralisation

Received: 16 February 2005 / Accepted: 25 May 2005 / Published online: 11 March 2006

Abstract Stratabound, uraniferous diagenetic xenotime cements provide a minimum depositional age of 1,632 ± 3 Ma for the sedimentary Birrindudu Group in the Killi Killi Hills, Tanami Region in northern Australia. The age of xenotime formation is broadly coeval with that recently proposed (1,650–1,600 Ma) for uranium mineralisation in the unconformity-associated deposits of the Pine Creek Inlier, northern Australia, and Athabasca Basin, Canada. The geological setting and formation model for the uraniferous xenotime crystals are similar to those widely proposed for unconformity-associated uranium deposits, suggesting a genetic link between the two. However, xenotime formation in the Birrindudu Group occurred during an apparently earlier stage of diagenesis, compared to late diagenetic formation of unconformity-associated uranium deposits. This could be explained by variations in the thickness of sediment cover and diachronous diagenesis across the basin, at the time of the basin-wide uranium mobilisation event, herein dated at ca. 1,630 Ma. In such a scenario, stratabound uraniferous xenotime cements could represent the remote distal zones of a more deeply buried, uranium mineralising system. Alternatively, the xenotime layer represents a precursor to, or a source for, later unconformity-associated ore deposition. In this case, the presence of diagenetic uraniferous xenotime in an area prospective for unconformity-associated uranium mineralisation would be an indication of, and still provide an approximate age for, uranium mobilisation within the cover sequence. Xenotime is a far more robust mineral than uraninite for U–Pb geochronology and can potentially provide a more reliable and precise timeframe for uranium mineralisation and subsequent recrystallisation events if present in the immediate uranium-ore environment.

Keywords Uraniferous xenotime · Unconformity-associated uranium · Diagenesis · U–Pb geochronology

Editorial handling: D. Huston

D. A. Vallini (✉) · D. I. Groves · N. J. McNaughton
I. R. Fletcher
Centre for Global Metallogeny, School of Earth and Geographic Sciences, University of Western Australia,
Crawley, WA, 6009, Australia
E-mail: Daniela.Vallini@woodside.com.au
Tel.: +61-8-64882773
Fax: +61-8-64881178

Introduction

Models and ages for the formation of unconformity-associated uranium deposits, notably those in the Athabasca Basin, Canada, and Pine Creek Inlier, Australia, have been much debated. Hoeve and Sibbald (1978) and Hoeve et al. (1980) discussed multiple models for the formation of the Canadian uranium deposits, from a magmatic-metamorphic, to diagenetic-hydrothermal or even supergene origin. However, a general consensus has evolved more recently in support of the following sequence of events in both the Athabasca and north Australian deposits (Maas 1989; Wilde et al. 1989; Solomon and Groves 1994; Ruzicka 1996):

1. Peneplanation and lateritic weathering of uranium-rich Archaean granitoid basement and Palaeoproterozoic sedimentary rocks;
2. Deposition of uranium-rich detritus in Mesoproterozoic basins;
3. Early diagenesis, resulting in some mobilisation of the uranium in the cover sequence;
4. Late diagenesis, with rapid subsidence and rifting in the basin resulting in the expulsion of oxidised sedimentary brines from thicker parts of the basin (Cathles and Smith 1983);
5. Circulation of oxidising fluids through the uranium-rich cover sequence, scavenging and mobilising uranium;
6. Circulation of some of the metalliferous fluids through syn-basinal faults and fracture zones, involving interaction with reductants in the units

below, or from reduced fluids derived from below, the unconformity;

7. Uranium mineralisation, and accompanying alteration, at the resultant redox front; and
8. Later period/s of hydrothermal fluid flow which resulted in the secondary remobilisation and re-deposition of uranium minerals, without significant change to ore-grade.

Fluid inclusion studies of altered and unaltered host rocks and hydrothermal quartz, calcite and dolomite from the Koongarra, Nabarlek and Jabiluka deposits, Pine Creek Inlier, indicate that temperatures were greater than 175°C and pressures were between 150 and 450 bars at the time of primary uranium mineralisation (Koul et al. 1988; Wilde et al. 1989). A geothermal gradient of approximately 100°C/km is suggested by Wilde et al. (1989). Deep burial (≥2 km depth) can provide the heat necessary to drive the ore-forming hydothermal circulation and removes the need for magmatic and other deep-seated heat sources (Johnston and Wall 1984), although not disproving possible contributions from such sources (Wilde et al. 1989).

Maas (1989) presented uraninite Sm–Nd and Rb–Sr ages of about 1,615 Ma (± 30 m y or greater), for the earliest phase of uraninite mineralisation in the deposits within the Alligator Rivers Uranium Field (see Fig. 1 for location). This corresponds to Rb–Sr sericite ages on ore zone rocks of 1,610 ± 40 Ma and 1,600 ± 80 Ma (Page et al. 1980) and Pb/Pb sulphide ages from an ore sample of 1,600 ± 150 Ma (Gulson and Mizon 1980), also within the Alligator Rivers Uranium Field. Younger ages of ca. 1,440 Ma (U–Pb whole-rock ages; Ludwig et al. 1987), 1,380–1,280 Ma (U–Pb, Pb/Pb uraninite and sulphide; Gulson and Mizon 1980), ca. 900 Ma (U–Pb pitchblende; Hills and Richards 1976) and 600–400 Ma (U–Pb whole-rock age; Ludwig et al. 1987) are thought by Maas (1989) to represent periods of recrystallisation of the initial uraninite during subsequent fluid-flow events. Uraniferous compounds from the Kylie Prospect in the south of the Rum Jungle Field yielded a primary intersection of the concordia at 1,627 ± 45 Ma and a secondary intersection at 232 ± 73 Ma (Von Pechmann 1986).

Cumming and Krstic (1992) considered that almost all uranium deposits in the Athabasca Basin, central Canada, formed in a restricted time interval between

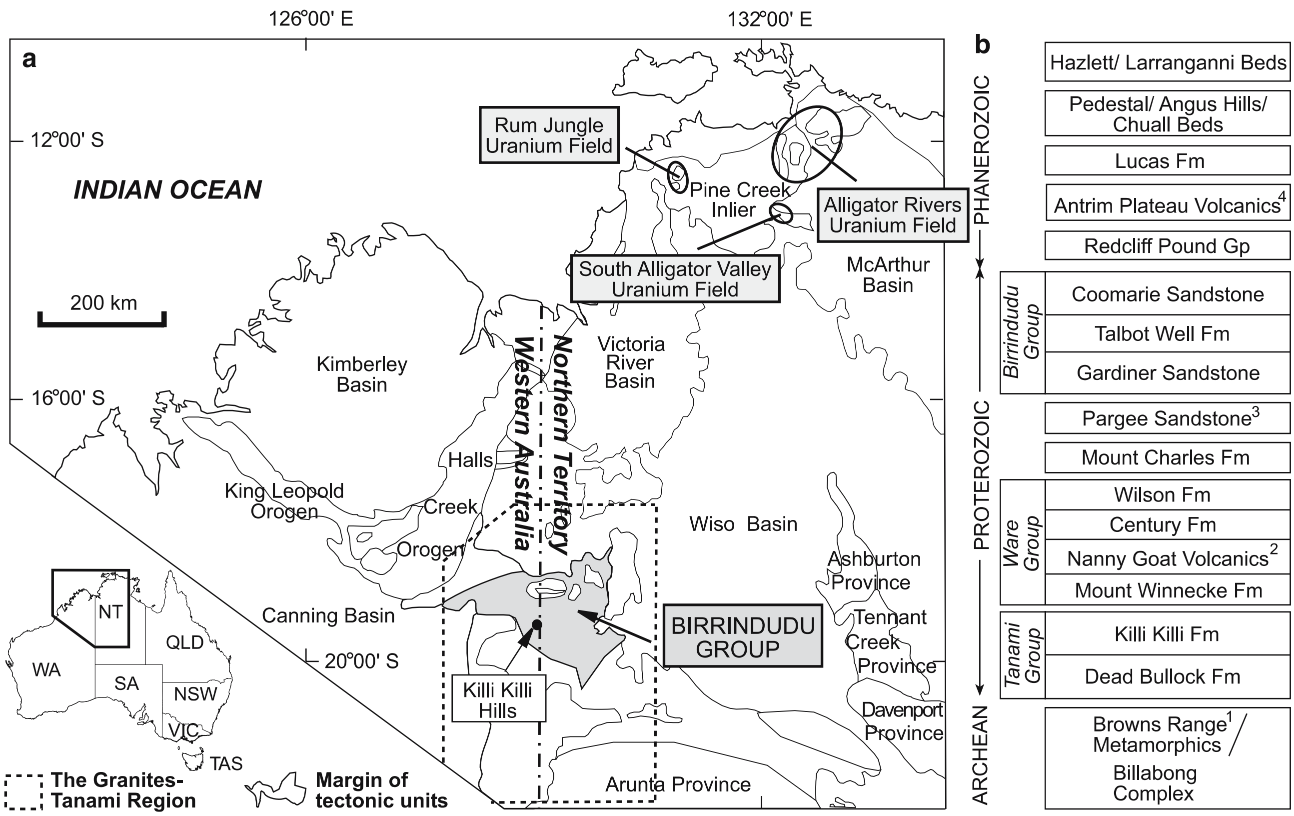

Fig. 1 **a** Locality map for the Proterozoic Birrindudu Group (*in grey*) within the Granites-Tanami Region on the Western Australia-Northern Territory border (modified from Hendrickx et al. 2002). The Killi Killi Hills are just west of the border. The uranium fields of the Pine Creek Inlier are also shown. **b** Schematic stratigraphic section showing the major rock units in the Granites-Tanami Region (based on Hendrickx et al. 2002). Granite suites (1,840–1,790 Ma; Page et al. 1995; Claoue-Long et al. 2001; Dean 2001; Smith 2001) intrude up to and including the Nanny Goat Volcanics. *Numbers* represent SHRIMP U–Pb ages-*1*, ca. 2,500 Ma (magmatic zircon; Page et al. 1995); *2*, ca. 1,815 Ma (magmatic zircon; Claoue-Long et al. 2001); *3*, 1,758 ± 15 Ma (detrital zircon; Crispe and Vandenberg 2005); *4*, 513 ± 12 Ma (magmatic zircon; Hanley and Wingate 2000)

about 1,360 Ma and 1,330 Ma. However, older ages of 1,477 ± 57 Ma (Rb–Sr in illite; Kotzer and Kyser 1990) and 1,521 ± 8 Ma (U–Pb in pitchblende; Cumming and Krstic 1992) have also been obtained from some of the deposits. Recent U–Pb and Ar/Ar dating of uraninite and clays from several deposits in the Athabasca Basin by Alexandre and Kyser (2003) indicates that pre-ore alteration sericite formed at 1,666 ± 6 Ma and that syn-ore coarse-grained sericite formed at 1,604 ± 48 Ma. The apparent large variation in age data (1,604 ± 48—ca. 1,330 Ma) for primary uranium mineralisation suggests that the younger ages, which are often interpreted as primary mineralisation ages, may be re-interpreted as Pb-loss or as uraninite recrystallisation ages.

The Granites-Tanami Region, straddling the Northern Territory-Western Australia border (Fig. 1), has many geological features in common with the Pine Creek Inlier and has consistently been considered highly prospective for uranium, as well as gold and the platinum group elements (Jagodzinski et al. 1992). The Gardiner Sandstone in the Granites-Tanami Region provides an extensive cover sequence whilst underlying units, the Davidson Beds and Antrim Plateau Volcanics, are enriched in Au–Pt–Pd–U in places. Crustal-scale fractures which transect the Archean basement and covering sequences could have provided structural controls for ore fluids. Uranium exploration in this region during the 1960–1970s identified anomalous radioactivity at two prospects in the Killi Killi Hills: No.1 and No.2 Prospects (Pritchard et al. 1960). The No.2 Prospect is about 11 km WNW of the No.1 Prospect. Both prospects are just west of the Northern Territory-Western Australia border (Fig. 1) and are in an area originally mapped by Traves et al. (1956) and Casey and Wells (1964).

The two radioactive zones occur in conglomerate beds in the basal 6 m of the Palaeoproterozoic Gardiner Sandstone, Birrindudu Group, which locally unconformably overlies the Killi Killi Formation. The No.1 Prospect, 1,350 m in length, and No.2 Prospect, 30 m in length, are assumed to be in the same horizon. Maximum radioactivity occurs at the eastern end of the No.1 Prospect. In the two prospects, Geiger counters recorded up to ten times background radioactivity, an average background reading being 0.02 mR/Hr (Pritchard et al. 1960). Deeply weathered rocks of the Killi Killi Formation directly underlying the anomalies have background levels of uranium, as do conglomerate beds higher in the sequence (Pritchard et al. 1960). Microscopic examination of samples from these two prospects by Pritchard et al. (1960) revealed that the radioactivity was not caused by U-minerals or ochres, but may be from what was tentatively identified as small crystals of xenotime and florencite within the matrix. A geochemical study by Jagodzinski et al. (1992) showed that arkoses from the Killi Killi Hills are depleted in Na_2O and CaO, which is characteristic of unconformity-style alteration (c.f. South Alligator uranium deposits), and is consistent with the circulation of oxidised, acidic basinal brines in the cover sequence.

In the present communication, new petrographic, age and chemical data are presented for the anomalous xenotime-rich zone in the Killi Killi Hills prospects. The purpose is to determine the relationship between unconformity-associated uranium deposits and the stratabound uraniferous xenotime cements and, in particular, whether they represent a potential source of uranium for this type of deposit, or a remote distal zone of such mineralisation, with associated exploration implications.

Geological background

The Granites-Tanami Region is an area of mainly Precambrian rocks covered by Cainozoic superficial sediments in the northwest of central Australia (Fig. 1a). A schematic stratigraphic section showing the major component rock units is depicted in Fig. 1b. The Birrindudu Group, mapped and described by Blake et al. (1972, 1973, 1979), comprises three conformable formations: the Gardiner Sandstone at the base, the dolomitic Talbot Wells Formation, and the Coomarie Sandstone at the top. Sedimentary structures, stromatolites and dolomite suggest deposition in shallow marine to intertidal environments on a stable continental margin (Clark and Blockley 1960). The Birrindudu Group is weakly metamorphosed and mildly deformed, and shows a marked angular unconformity with underlying formations, which are deeply weathered, commonly multiply deformed and metamorphosed to greenschist and locally amphibolite facies. It rests unconformably on the Browns Range Metamorphics, Tanami Group, Ware Group and Pargee Sandstone (Crispe and Vandenberg 2005). The Birrindudu Group also unconformably overlies intrusions of the uranium-rich ca. 1,815 Ma Coomarie Dome (Smith 2000), ~35 km to the east of the Killi Killi Hills, which shows evidence of ongoing uplift after deposition of the Birrindudu Group (Hendrickx et al. 2000). Sediments in the Gardiner Sandstone may have been derived from the underlying Tanami and Ware Groups as well as the granite suites, with some contribution from Neo-Archean rocks (Crispe and Vandenberg 2005). There is an unconformity between the Birrindudu Group and overlying units. Blake et al. (1979) gave a maximum thickness of 6 km for the Birrindudu Group east of the Gardiner Range, 30-40 km NNE of the Killi Killi Hills. However, on the northern margin of the Coomarie Dome, 50–60 km ENE of the Killi Killi Hills, a section through the Group has a total thickness of only 1.9 km (Hendrickx et al. 2000). The Birrindudu Group exhibits fault-propagated folding during deformation after ca. 513 Ma (Vandenberg et al. 2001).

The age of the Birrindudu Group is not well constrained. It is bracketed between 1,758 ± 15 Ma, the age of the youngest detrital zircon population in the underlying Pargee Sandstone (Crispe and Vandenberg 2005), and 513 ± 12 Ma, the age of the overlying Antrim

Plateau Volcanics (U–Pb zircon; Hanley and Wingate 2000: Fig. 1b). In the Victoria River Region (Fig. 1a), rocks in drill-core that are interpreted to be equivalent to the Birrindudu Group are overlain by the Limbunya Group (Crispe and Vandenberg 2005). Tuffaceous horizons in the Limbunya Group have been dated at 1,636 ± 5 Ma and 1,639 ± 7 Ma (U–Pb zircon; Smith 2001).

The Gardiner Sandstone in the Killi Killi Hills section represents filled channels in old basement consisting of deeply weathered, turbiditic Killi Killi Formation locally intruded by 1,820–1,790 Ma granitoids (Clark and Blockley 1960; Smith 2001). The basal conglomerate beds consist of numerous interlocking lenses of highly silicified grit, pebbly sandstone and conglomerate. This grades into medium to thick bedded, medium-grained sublithic to lithic arenite and quartz arenite. Thinly bedded, fine-grained quartz greywacke, shale and siltstone in the middle of the formation are subordinate. The conglomerate and pebbly sandstone samples analysed in this study are clast-supported and mainly comprise well-rounded sand- to pebble-size quartz grains with well-preserved syntaxial quartz overgrowths. There are lesser amounts of lithic clasts (up to 3 cm long) composed of vein quartz, lithic arenite, greywacke, siltstone, shale and chert which are rimmed by hematitic clays. There are also small amounts of hydrated iron (Fe) oxide, hematitic clays and Fe-stained phosphates in the matrix.

Analytical techniques

Nine hand-size specimens (sample ID = 92496002-004, 92496018-022) of surface samples of the basal conglomerate from two localities in the Killi Killi Hills (7,813,177 mN, 498,360 mE; 7,813,398 mN, 497,016 mE), as studied by Jagodzinski et al. (1992), were supplied by Geoscience Australia. Polished thin sections were cut and examined by polarising microscope and high-resolution backscattered scanning electron (BSE) microscopy on a JEOL JSM-6400 Scanning Electron Microscope (SEM), equipped with a Link Systems energy dispersive X-ray microanalyser used for qualitative analysis. Operating conditions were 15–20 kV accelerating voltage and 3 nA beam current.

Uranium–Pb data were collected from xenotime crystals located in thin sections, using a sensitive high resolution ion microprobe (SHRIMP). Three-millimetre diameter plugs containing selected xenotime crystals were drilled out of polished thin sections and mounted in epoxy resin disks (mounts UWA C-72, C-73, C-117 and C-118) for in situ analysis. Separate standard mounts were cleaned and gold coated simultaneously with the sample mounts prior to analysis. The primary Pb–U standard used was MG-1; the secondary standards were BS-1, which monitors matrix corrections, and XENO-1 which monitors both matrix corrections and ^{207}Pb/^{206}Pb (Fletcher et al. 2004). SHRIMP analytical procedures and matrix corrections for REE, U and Th, follow those published in Fletcher et al. (2000, 2004). Uncertainties in the tabulated and plotted data include all identified sources of random error, and are quoted at 1σ, whereas ages from pooled data are quoted with 95% confidence limits. All ages quoted in text and figures are ^{207}Pb/^{206} Pb ages.

Xenotime crystals were analysed for Si, P, Ca, Fe, Y, Zr, REE, Pb, Th and U using a JEOL 6400 SEM equipped with a wavelength dispersive (WDS) analyser. Operating conditions were 20 kV, 100 nA on a Faraday cup, 40° take-off angle and an analysis resolution of 3 μm. Peak overlap correction factors were applied to counteract REE emission peak overlaps during measurements. Metals, synthetic silicate and REE glasses were used for calibration. The detection limits were 0·003 wt% for Si and Ca, 0·038 wt% for P, 0·017 wt% for Fe, 0·019 wt% for Y, 0·01 wt% for Zr, ~0·015 wt% for REE, 0·018 wt% for Pb and 0·08 wt% for Th and U. Chemical formulae were calculated on the basis of four oxygens. Only those results with oxide totals of 98·0–102·0 wt%, cation structural totals of 1·98–2·02 (for four oxygens) and < 1·0 wt% ZrO_2(to avoid analyses which overlapped zircon) were accepted as reliable analyses.

Description of authigenic xenotime

Authigenic xenotime, in a variety of forms, comprises up to ~30% of the matrix of the conglomerate samples. All xenotime crystals show varying degrees of weathering, with many too fractured to enable analysis (see Fig. 2a). Hematitic clays occur as sub-micron inclusions within xenotime crystals, as well as in quartz cement. The clays are probably the products of weathering of precursor Fe-alteration minerals. Chemical zonation in xenotime crystals is rare in BSE images, although textural variations across crystals are common, involving abrupt changes from massive to pitted xenotime (Fig. 2b), suggesting the presence of multiple xenotime generations within single crystals, some of which may have been partly dissolved. Texturally oldest xenotime occurs as irregular and pyramidal overgrowths on detrital zircon grains, and as strings of minute subhedral crystals which line detrital quartz-grain surfaces. A brief description of the different forms of xenotime is presented here.

Pyramidal xenotime overgrowths on detrital zircon grains (Fig. 2c) have planar crystal edges that form a pseudo-pyramidal habit (c.f. Rasmussen 1996). The overgrowths generally measure ≤ 60 μm in length from base to tip. Pore-filling quartz cements surround and preserve the euhedral boundaries of the pyramidal xenotime overgrowths (Fig. 2a), suggesting that overgrowths formed prior to diagenetic quartz cementation.

Irregular xenotime overgrowths, similar to those described by Vallini et al. (2002), occur as cement-like overgrowths, up to 200 μm in diameter, which surround detrital zircon grains (Fig. 2d). The overgrowths commonly fill most of the pore space, causing irregular

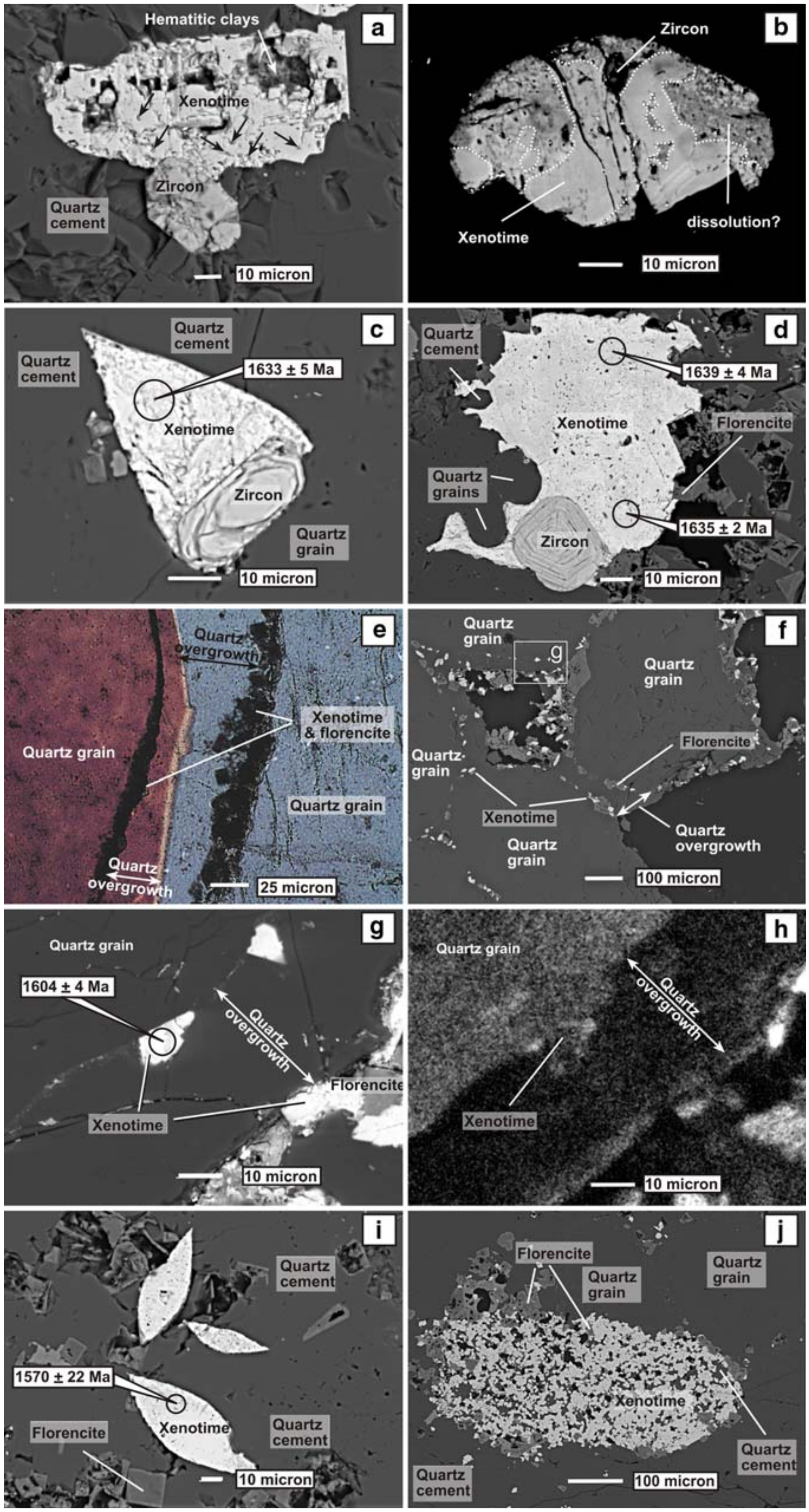

Fig. 2 Backscattered electron (*BSE*) images of authigenic xenotime crystals within the Gardiner Sandstone. SHRIMP analysis spots are labelled. **a** Xenotime overgrowth on detrital zircon grain showing fractures and hematitic clay inclusions associated with weathering (*black arrows*). **b** Xenotime overgrowth on detrital zircon grain showing textural variations across the crystal suggesting partial dissolution and the presence of multiple xenotime generations (outlined by *dashed white lines*). **c** Pseudo-pyramidal xenotime overgrowth on detrital zircon grain surrounded by quartz cement (mount C117, grain G). **d** The rim of the large cement-like xenotime overgrowth on detrital zircon grain preserves the outlines of detrital quartz grains, euhedral florencite grains, and some quartz cement faces (mount C118, grain F). **e** Thin layers of Fe-stained phosphates line quartz grain surfaces (mount C118). **f** Boundary between detrital quartz grains and their syntaxial quartz overgrowths defined by strings of xenotime and florencite crystals and clays (mount C118): the area pictured in (**g**) is outlined. **g** Close-up of the area outlined in (**f**) (mount C117, grain M). **h** (*CL*) image of the xenotime crystal in (**g**), with the boundary between the detrital quartz grain (*light grey*) and its syntaxial quartz overgrowth (*dark grey*) clearly defined. **i** Large leaf-shaped xenotime crystals surrounded by quartz cement (mount C72, grain 17c). **j** Intra-clast with its matrix replaced by small euhedral xenotime crystals and pseudo-cubic florencite crystals (mount C72)

boundaries where they impinge on surrounding grains such as detrital quartz grains and euhedral florencite crystals (Fig. 2d). Diagenetic quartz cement surrounds most overgrowth boundaries and thus post-dates the majority of xenotime formation. However, part of the rim of the overgrowth in Fig. 2d preserves the outline of

Table 1 SHRIMP data for authigenic xenotime in the Gardiner Sandstone

Analysis Spot[a]	U (ppm)	Th (ppm)	Th/U	f206 (%)[b]	$^{207}Pb/^{206}Pb$	±[c]	$^{206}Pb/^{238}U$	±	$^{207}Pb/^{235}U$	±	$^{207}Pb/^{206}Pb$ Conc. (%)[d]	$^{207}Pb/^{206}Pb$ Age (Ma)	±	Xenotime type[e]
C118.F1-1	25,000	332	0.01	0.004	0.1008	0.0002	0.2753	0.0072	3.828	0.100	96	1,639	4	z
C72.12b-1	398	239	0.60	0.000	0.1006	0.0014	0.2690	0.0066	3.732	0.106	94	1,636	26	z
C118.F1-2	19,100	4,129	0.22	0.007	0.1006	0.0001	0.2572	0.0066	3.566	0.091	90	1,635	2	z
C117.E1-1	23,900	160	0.01	0.003	0.1005	0.0001	0.2810	0.0073	3.895	0.100	98	1,634	3	z
C117.G1-1	19,000	1,778	0.09	0.022	0.1005	0.0003	0.2370	0.0059	3.283	0.082	84	1,633	5	z
C117.H1-1	25,400	796	0.03	0.005	0.1005	0.0002	0.2554	0.0067	3.538	0.093	90	1,632	3	z
C118.B1-1[2]	18,200	907	0.05	0.007	0.1001	0.0004	0.2888	0.0136	3.987	0.188	101	1,626	7	z
C117.B1-1	23,700	363	0.02	0.005	0.1001	0.0002	0.2664	0.0069	3.677	0.095	94	1,626	4	z
C118.D1-1[2]	29,800	862	0.03	0.006	0.0998	0.0002	0.2305	0.0120	3.173	0.165	82	1,621	5	z
C72.14d-2	459	142	0.31	0.000	0.0997	0.0010	0.2874	0.0066	3.952	0.098	101	1,619	19	z
C72.6b-1	789	45	0.06	0.290	0.0993	0.0012	0.2257	0.0048	3.091	0.075	81	1,611	22	z
C117.M1-1	22,000	423	0.02	0.014	0.0989	0.0002	0.2357	0.0060	3.215	0.082	85	1,604	4	q
C73.7B-2	2780	69	0.02	0.418	0.0988	0.0015	0.3132	0.0065	4.268	0.112	110	1,602	29	q
C118.D2-1[2]	27,800	1,345	0.05	0.007	0.0987	0.0003	0.2237	0.0115	3.046	0.156	81	1,600	5	q
C118.H2-1	1,960	44	0.02	0.672	0.0986	0.0013	0.2331	0.0053	3.170	0.083	85	1,598	24	q
C118.A2-2[2]	25,600	1,369	0.05	0.008	0.0985	0.0003	0.2274	0.0114	3.089	0.150	83	1,596	5	z
C118.O1-1[2]	297	842	2.83	0.794	0.0985	0.0028	0.2758	0.0122	3.744	0.198	98	1,595	53	z
C73.3B-1	1,600	81	0.05	0.529	0.0984	0.0015	0.2437	0.0050	3.306	0.086	88	1,594	29	q
C118.O1-2[2]	1,240	697	0.56	0.187	0.0983	0.0008	0.2437	0.0105	3.302	0.145	88	1,591	16	z
C73.7B-1	1,230	61	0.05	0.237	0.0982	0.0011	0.3214	0.0067	4.351	0.103	113	1,590	21	q
C118.M1-1[2]	505	128	0.25	0.447	0.0981	0.0013	0.3220	0.0136	4.356	0.194	113	1,588	25	z
C117.O1-1	17,900	2,277	0.13	0.008	0.0973	0.0003	0.2201	0.0056	2.954	0.076	82	1,573	5	z
C72.17c-1	782	620	0.79	0.245	0.0971	0.0011	0.2989	0.0067	4.004	0.101	107	1,570	22	r
C118.P1-1[2]	18,000	425	0.02	0.016	0.0969	0.0003	0.2214	0.0104	2.959	0.139	82	1,566	5	z
C118.K1-1[2]	21,700	1,602	0.07	0.011	0.0966	0.0003	0.2364	0.0115	3.149	0.154	88	1,560	5	z
C72.17a-1	1,039	157	0.15	0.189	0.0959	0.0008	0.2832	0.0064	3.744	0.090	104	1,546	15	r
C118.A2-1[2]	25,900	727	0.03	0.006	0.0959	0.0003	0.2361	0.0119	3.121	0.158	88	1,545	7	z
C73.11C-1	890	567	0.64	0.710	0.0954	0.0021	0.2230	0.0046	2.934	0.088	84	1,537	41	z
C72.3a-1	293	91	0.31	0.670	0.0954	0.0034	0.3090	0.0083	4.066	0.182	113	1,537	68	z
C72.15a-1	9,200	279	0.03	0.013	0.0936	0.0003	0.2041	0.0042	2.635	0.055	80	1,501	6	r
C72.11a-1	490	173	0.35	0.473	0.0923	0.0014	0.2368	0.0055	3.015	0.084	93	1,475	29	r
<80% concordance														
C118.I1-1	1,910	30	0.02	0.262	0.1004	0.0007	0.2075	0.0052	2.872	0.074	75	1,631	12	z
C117.F3-1	21,400	1,039	0.05	0.008	0.0992	0.0003	0.2146	0.0054	2.934	0.075	78	1,608	5	z
C118.O1-3[2]	374	831	2.22	0.287	0.0992	0.0014	0.2065	0.0091	2.823	0.130	75	1,608	26	z
C73.9B-1	630	354	0.56	0.335	0.0987	0.0017	0.1594	0.0035	2.170	0.061	60	1,600	32	z
C73.15A-1	1,074	402	0.37	0.323	0.0977	0.0013	0.1915	0.0041	2.581	0.065	71	1,581	25	z
C73.9A-1	832	124	0.15	0.585	0.0976	0.0022	0.1320	0.0063	1.777	0.094	51	1,579	43	z
C117.L1-1	16,800	1,530	0.09	0.012	0.0976	0.0001	0.2059	0.0050	2.771	0.067	76	1,579	3	z
C117.F3-2	20,000	584	0.03	0.009	0.0975	0.0003	0.2111	0.0056	2.838	0.076	78	1,577	7	z
C117.F1-1	19,000	3,651	0.19	0.009	0.0973	0.0001	0.1776	0.0045	2.384	0.060	67	1,574	3	z
C118.A1-2[2]	26,300	508	0.02	0.012	0.0967	0.0003	0.1934	0.0098	2.578	0.131	73	1,561	7	r
C118.A1-3[2]	27,200	113	0.00	0.009	0.0964	0.0002	0.1936	0.0098	2.574	0.130	73	1,556	4	r
C118.N1-1[2]	27,800	2,822	0.10	0.010	0.0964	0.0003	0.1792	0.0092	2.381	0.123	68	1,555	6	z
C118.H1-1	1,900	28	0.02	0.327	0.0958	0.0008	0.1952	0.0045	2.579	0.063	74	1,544	15	z
C72.17b-2	688	453	0.66	0.223	0.0957	0.0014	0.1922	0.0041	2.537	0.070	73	1,543	27	z
C118.A1-1[2]	24,400	1,244	0.05	0.011	0.0953	0.0003	0.2013	0.0100	2.645	0.131	77	1,533	6	r
C117.G1-2	15,800	229	0.01	0.021	0.0951	0.0003	0.2031	0.0049	2.663	0.065	78	1,530	5	z
C72.18a-1	40,300	254	0.01	0.077	0.0946	0.0008	0.0486	0.0015	0.633	0.022	20	1,520	17	z
C117.F2-1	20,100	3,172	0.16	0.018	0.0943	0.0007	0.1348	0.0036	1.752	0.050	54	1,514	14	z
C118.G1-1	19,200	1,775	0.09	0.005	0.0942	0.0003	0.1696	0.0045	2.203	0.058	67	1,513	6	z
C118.F1-3[2]	29,000	713	0.02	0.010	0.0933	0.0008	0.1711	0.0089	2.201	0.120	68	1,493	16	z
C117.N1-1	15,200	463	0.03	0.014	0.0927	0.0005	0.1369	0.0033	1.750	0.043	56	1,481	10	r
C117.K1-1	23,100	226	0.01	0.011	0.0926	0.0006	0.1488	0.0039	1.900	0.052	60	1,479	13	z
C117.I1-1	18,200	1,783	0.10	0.017	0.0921	0.0007	0.1631	0.0041	2.073	0.055	66	1,470	15	z
C118.E1-2[2]	30,800	579	0.02	0.131	0.0914	0.0007	0.0375	0.0020	0.472	0.025	16	1,454	15	r
C117.N1-2	16,000	477	0.03	0.033	0.0902	0.0002	0.1360	0.0033	1.692	0.041	57	1,430	3	r
C118.E1-1	19,800	478	0.02	0.098	0.0896	0.0003	0.0753	0.0019	0.930	0.023	33	1,417	6	r
C118.E1-3[2]	31,000	576	0.02	0.072	0.0887	0.0003	0.0369	0.0019	0.451	0.024	17	1,397	7	r
C72.14a-1	9,980	749	0.08	0.064	0.0828	0.0004	0.1171	0.0032	1.336	0.037	56	1,264	9	z
C72.8a-1	11,000	349	0.03	0.046	0.0761	0.0004	0.0979	0.0019	1.027	0.021	55	1,097	11	z
C72.12a-1	11,800	334	0.03	0.189	0.0751	0.0011	0.0950	0.0018	0.983	0.025	55	1,070	31	z
C72.14a-2	16,600	1,240	0.07	0.688	0.0732	0.0021	0.0764	0.0016	0.772	0.030	47	1,020	58	z

Table 1 (Contd.)

>1% f206														
C73.13A-1	1,270	135	0.11	5.902	0.1036	0.0067	0.2684	0.0064	3.832	0.265	91	1,689	119	z
C72.17b-1	630	538	0.85	4.550	0.1025	0.0048	0.2200	0.0050	3.109	0.162	77	1,670	86	z
C72.14d-1	797	113	0.14	1.281	0.0989	0.0020	0.2799	0.0077	3.816	0.129	99	1,603	37	z
C73.10E-1	1,820	105	0.06	4.676	0.0954	0.0224	0.2847	0.0076	3.745	0.897	105	1,536	443	z
C73.16A-1	3,430	72	0.02	1.055	0.0883	0.0024	0.0628	0.0025	0.765	0.037	28	1,389	52	r
C73.9A-2	3,160	246	0.08	2.036	0.0860	0.0036	0.0444	0.0009	0.526	0.025	21	1,337	80	z
C73.16A-2	5,500	82	0.01	1.595	0.0852	0.0022	0.0542	0.0011	0.637	0.021	26	1,320	50	r

Data are listed in $^{207}Pb/^{206}Pb$ age order, and those with <80% concordance or >1% f206 are listed separately

[a] Mounts C-72 and C-73 were analysed on 13/10/2002, C-117 was analysed on 18/01/2003 and C-118 was analysed on 18/01/2003 and 07/02/2003. Analysis spot number and letter following the decimal point (.) refer to the grain identification and the number following the dash (-) refers to the analysis number for that grain. [2] = C118 analyses from the second session

[b] f206(%) = % of ^{206}Pb which is due to common Pb; All listed Pb isotope data are corrected for common Pb, using measured ^{204}Pb and the composition of Broken Hill galena

[c] Precisions are 1σ; U/Pb systematic reproducibility propagated from MG-1 standards for Mount C-72 and C-73 is 1.7 % ($n=14$), for Mount C-117 and Mount C-118 (1st session) is 2.0 % ($n=4$) and for Mount C- 118 (2nd session) is 3.9% ($n=7$)

[d] % concordance, as 100 x [t($^{206}Pb/^{238}U$)/t($^{207}Pb/^{206}Pb$)]

[e] *z* xenotime associated with zircon; *q* xenotime associated with quartz cement; *r* xenotime replacement of grains/clasts

euhedral quartz cement faces. This suggests that there are multiple generations of xenotime within this crystal which formed both pre- and post- diagenetic quartz cementation.

Strings of minute subhedral xenotime crystals (≤ 10 μm) line the surfaces of detrital quartz grains and are engulfed by well-preserved (≤ 150 μm-long) syntaxial quartz overgrowths (Fig. 2e, f), placing the timing of formation of these xenotime crystals pre- to syn-diagenetic quartz cementation. There is no associated zircon, but some florencite crystals and clay material are present. Figure 2g, h shows, the same field of view, with the cathodoluminescence image (Fig. 2h) highlighting the boundary between the detrital quartz grain and syntaxial quartz overgrowth.

Other morphological types of xenotime include large (50–200 μm in length) leaf-shaped crystals (Fig. 2i) and patchy cements (Fig. 2j) consisting of ≤ 10 μm euhedral crystals which have amalgamated and replaced rounded lithoclasts and pockets of the original matrix material. Neither have associated zircon and, in places, they appear to be intergrown with and engulfing diagenetic quartz cement. They are texturally younger than the types described above and formed by the replacement of other grains and clasts.

SHRIMP U–Pb age data

Age data from the SHRIMP analysis of 51 xenotime crystals are listed in $^{207}Pb/^{206}Pb$ age order in Table 1. Some xenotime overgrowths had multiple analysis spots placed on them, but there were no multiple analyses in any analysis spot. A few of the corresponding analysis locations are shown in Fig. 2. Seven of the 69 analyses contained >1 wt% common lead (f206) and are not discussed further; the remainder of the data have low to negligible f206.

Discordance

After following standard procedures by applying matrix corrections to the raw data (Fletcher et al. 2000, 2004), it was apparent that the scatter in U/Pb ratios increased when matrix corrections were applied, particularly in those analyses with very high uranium values which had shifts in "apparent" discordance of up to 26%. The chemical composition of the xenotime in the Gardiner Sandstone is unusual, not only for its high U but also high Fe-contents (Table 2). This probably relates to the state of weathering of the samples studied, reflected by the degree of Fe-staining and abundance of secondary mineral inclusions in most of the analysed areas (Fig. 2a). The effect of Fe, and potentially related elements, on the relative ionisation efficiencies of U^+ and Pb^+ in SHRIMP has not been assessed by previous studies, which attempted to quantify the corrections on U/Pb due to variable concentrations of U, Th and REE in massive xenotime (Fletcher et al. 2000, 2004). Thus, the true U–Pb concordance of these samples is largely unknown. Despite this, it is argued that the $^{207}Pb/^{206}Pb$ data are valid. Lead-loss, normally associated with metamorphism in zircon studies, has not occurred in this case as the Gardiner Sandstone samples are virtually unmetamorphosed. Xenotime may have been partially dissolved during subsequent hydrothermal activity or weathering, but there is no evidence for Pb-leaching under these conditions. Nonetheless, all analyses with >20% "apparent" discordance are omitted from the discussion.

Age populations

The $^{207}Pb/^{206}Pb$ data are displayed in a probability plot in Fig. 3a. To determine whether the peaks represent discrete age populations or are age mixtures, it was necessary to examine the ages recorded in each textural

Table 2 Geochemical data for several xenotime crystals in the Gardiner Sandstone

This study											Xenotime standards[a]			MountBarren Group[b]	
Maximum						Average					Average			Average	
GRAIN	C117G	C117B	C118O	C118M	C72I	C117G	C117B	C118O	C118M	C72I	BS-1	MG-1	Xeno-1	Early Diagenetic	Diagenetic
Spot ID.	6	5	3	1	6										
n(spots)						15	7	5	3	8	21	18	20	25	28
Oxide (wt%)															
SiO2	0.00	0.13	0.45	0.00	0.32	0.13	0.24	0.15	0.00	0.13	0.14	0.00	0.61	1.07	0.67
P2O5	36.02	33.77	33.72	33.31	30.17	35.43	34.51	34.81	34.20	32.49	33.64	36.05	35.33	35.23	36.33
CaO	1.12	0.88	0.19	0.09	0.12	0.83	0.85	0.18	0.09	0.11	0.02	0.03	0.03	0.59	0.29
FeO	2.71	3.47	4.95	6.74	10.28	0.74	1.25	1.93	4.00	5.12	0.00	0.00	0.00	0.16	0.08
Y2O3	47.68	41.67	42.24	40.31	39.52	44.29	42.53	43.81	41.57	42.46	41.18	45.70	42.89	47.41	45.99
ZrO2	0.00	0.00	0.00	0.00	0.52	0.00	0.00	0.00	0.00	0.61	0.55	0.70	0.94	0.10	0.55
Σ REE	12.83	16.59	16.93	18.13	18.07	17.37	17.54	19.03	19.06	19.35	20.08	15.72	18.27	14.58	15.34
PbO2	0.06	0.17	0.00	0.00	0.00	0.15	0.37	0.00	0.00	0.01	0.00	0.00	0.00	0.04	0.29
Th2O3	0.04	0.05	0.10	0.06	0.03	0.12	0.08	0.09	0.04	0.03	0.44	0.12	0.31	0.07	0.01
U2O3	1.79	2.68	0.11	0.12	0.03	2.23	3.16	0.11	0.10	0.05	0.10	0.16	1.78	0.67	0.31
Total	101.59	98.91	98.13	98.02	99.06	101.29	100.53	100.11	99.06	100.36	96.00	98.31	100.12	99.92	99.86

Single analyses (from each crystal) which have the maximum FeO content are listed separately to the set of average values given for each crystal. Reference data: [a] Fletcher et al. (2004), [b] Vallini et al. (2005)

type of xenotime: xenotime associated with zircon, xenotime associated with syntaxial quartz overgrowths, and xenotime which had replaced other minerals. The probability plots in Figs. 3b–d show the ages recorded by each of the three xenotime types. Figure 3e contains combined ages for the xenotime associated with zircon and replacement xenotime. It is apparent that the peak at ca. 1,630 Ma is only recorded in xenotime associated with zircon (Fig. 2c, d) and, since it forms the maximum end of the dataset, it cannot be an age mixture. Eleven analyses from this xenotime type give a weighted mean age of 1,632 ± 3 Ma (MSWD = 1.6). This population is presented as a concordia plot in Fig. 4.

Most significantly, however, is that the six analyses from the minute xenotime crystals that line detrital quartz grains, and are engulfed by syntaxial quartz overgrowths (Fig. 2e), record a single age population at ca. 1,600 Ma (Fig. 3c). They record a discrete xenotime growth event, and were sealed off from further xenotime growth or subsequent dissolution by the formation of the syntaxial quartz overgrowths. This age has also been recorded in a few analyses of xenotime associated with zircon (Fig. 3b) but not in the replacement xenotime (Fig. 3d). If the six analyses from the xenotime associated with quartz cement are considered a population, the weighted mean age is 1,602 ± 6 Ma (MSWD = 0.19).

The apparent peak at ca. 1,560 Ma is recorded in the xenotime associated with zircon (Fig. 3b) and within the replacement xenotime (Fig. 2g, 3d). Since it is the first time the replacement xenotime appears in the age dataset, this peak may represent a discrete xenotime growth event. If these analyses are considered to be a population, the weighted mean age is 1,563 ± 8 Ma ($n = 9$; MSWD = 1.9). However, the analyses may actually represent age mixtures so, to avoid over-interpretation of a relatively small dataset, the xenotime growth event is considered as ca. 1,560 Ma. There is some evidence of xenotime growth at ca. 1,500–1,480 Ma recorded in both the xenotime associated with zircon and the replacement xenotime.

A statistical mixture modelling program embedded in Isoplot (Sambridge and Compston 1994) was applied to the total dataset. This identifies age groupings at 1,633 ± 4 Ma ($n = 9$; MSWD = 1.8), 1,602 ± 5 Ma ($n = 8$; MSWD = 0.41) and 1,564 ± 8 Ma ($n = 12$; MSWD = 1.9), indistinguishable from the weighted mean averages defined above.

Interpretation

The most reliable petrographic constraint for the timing of the ca. 1,630 Ma xenotime generation within the diagenetic realm is its relationship to diagenetic quartz cement. Diagenetic quartz cement is defined by Morad et al. (2000) as being one of the most important permeability and porosity-reducing alteration products in deeply-buried sandstones during the latter stages of diagenesis. The syntaxial quartz overgrowths surrounding detrital quartz grains in these rocks must have formed at the same time as, or soon after, the ca. 1,600 Ma xenotime crystals that they enclose. Thus, the ca. 1,630 Ma xenotime generation formed prior to late diagenesis, although it is not known how much earlier. The 1,632 ± 3 Ma maximum xenotime age provides a minimum age of sedimentation for the Gardiner Sandstone and burial of the underlying unconformity. The concentration of xenotime ages around ca. 1,560 Ma possibly record a subsequent hydrothermal fluid flow event. Interestingly, this age is consistent with K–Ar and Rb–Sr glauconite ages of 1,560 ± 20 Ma and 1,560 ± 120 Ma (Page et al. 1976) from samples of the

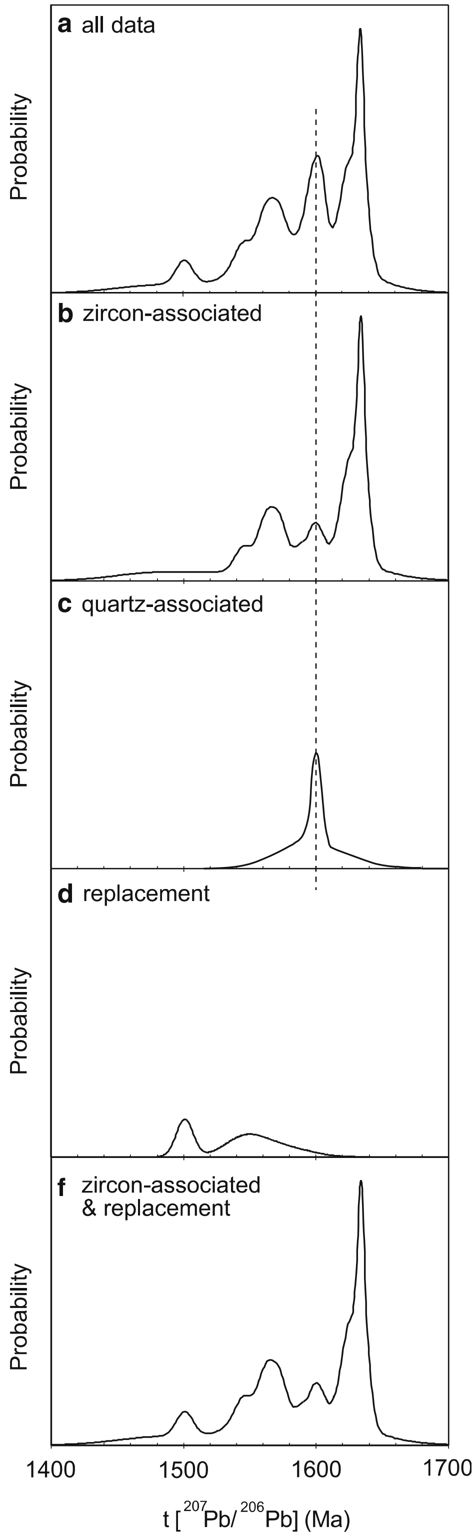

Fig. 3 a Cumulative probability curve of data from all three xenotime types; the dashed line indicates the ca. 1,600 Ma population. **b** Cumulative probability curve for xenotime associated with zircon. **c** Cumulative probability curve for xenotime associated with syntaxial quartz overgrowths. **d** Cumulative probability curve for replacement xenotime. **e** Cumulative probability curve for combined xenotime associated with zircon and replacement xenotime

Gardiner Sandstone. Page et al. (1976) interpreted these ages as recording the last time the sediments cooled below the closure temperature of glauconite. This resetting of glauconite at ca. 1,560 Ma, as well as coincident hydrothermal xenotime growth, possibly records hydrothermal activity in the Granites-Tanami Region associated with the Chewings Orogeny (1,590–1,570 Ma) in the Arunta Region.

Xenotime uranium chemistry

SHRIMP analysis reveals very high uranium concentrations within a large number of the xenotime crystals (Tables 1, 2). Thirty eight of the total 69 analyses have uranium concentrations >1.0 wt% and 22 have >2.0 wt% U, the highest being 4.0 wt%. Eight of the 11 analyses of the ca. 1,630 Ma diagenetic xenotime population have uranium concentrations between 2 and 3 wt%. In comparison, diagenetic xenotime crystals from Palaeoproterozoic sandstones of the Mount Barren Group in southern Western Australia have uranium concentrations of 0.07–0.85 wt% (Vallini et al. 2002), those from the Warton Sandstone and Pentecost Sandstone in the Kimberley region, Western Australia, have uranium values of 0.14–0.40 wt% and 0.02–0.14 wt%, respectively (McNaughton et al. 1999), diagenetic xenotime crystals in the Stirling Range Formation, southern Western Australia have values of 0.13–0.30 wt% U (Rasmussen et al. 2004), and those from the uranium-rich Witwatersrand Basin, South Africa, have values of 0.25–1.0 wt% U (Kositcin et al. 2003), some of which is attributed to sub-micron uraninite inclusions within the xenotime crystals.

Anomalously high uranium concentrations also characterise some of the xenotime crystals with younger ages (Table 1). This suggests that, after the initial introduction of large amounts of uranium into the basal Gardiner Sandstone and incorporation into xenotime during diagenesis, some reworking of the earliest generation of xenotime occurred during the growth of successive xenotime generations. Textural and geochronological evidence (Fig. 2b) suggest that the earliest generation of xenotime, which nucleated on zircon grains, was partially dissolved and re-precipitated as cements with no associated zircon or as additions to earlier-formed xenotime overgrowths on zircons. The same process of successive dissolution and re-deposition at essentially constant uranium concentrations is considered to have occurred within major unconformity-associated uranium deposits (e.g. Maas 1989; Kotzer and Kyser 1990). The fact that some of the analyses, regardless of age, have markedly lower uranium concentrations (i.e. <1 wt%) suggests that there may have been two sources of uranium at the time of xenotime formation, with the high uranium source only accessed in the initial stage of xenotime formation.

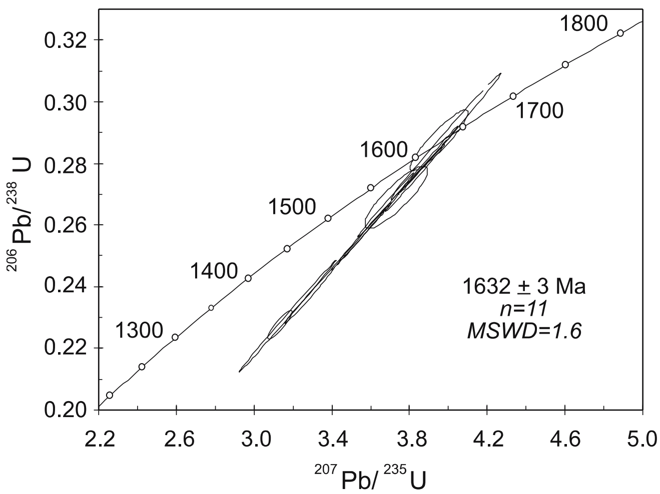

Fig. 4 Uranium–Pb concordia diagram for the oldest xenotime population at ca. 1,630 Ma

Discussion

Comparison with unconformity-associated uranium deposits

There are striking similarities between the uraniferous xenotime cement horizon in the Killi Killi Hills area and the unconformity-associated uranium deposits in the Pine Creek Inlier and Athabasca Basin in terms of their geological setting, diagenetic-hydrothermal formation processes, age of burial of the associated unconformity and age of mineralisation.

The geological setting of the uraniferous xenotime horizon in the Killi Killi Hills area is comparable to that of the uranium deposits (see Maas 1989; Wilde et al. 1989; Solomon and Groves 1994; Ruzicka 1996) and the Gardiner Sandstone contains alteration signatures similar to that accompanying unconformity-associated uranium mineralisation (Jagodzinski et al. 1992). The only feature that appears to be lacking from a typical ore zone is a basement fault or shear zone, invoked in most genetic models, to channel reduced fluids from the basement (e.g. Hoeve and Sibbald 1978; Hoeve et al. 1980; Maas 1989; Wilde et al. 1989; Solomon and Groves 1994; Ruzicka 1996). However, the strike of the elongate No. 1 Prospect uranium-anomaly is parallel to an E–W fault, about 150 m to the south of the prospect, which displaces the Gardiner Sandstone (Jagodzinski et al. 1992). This could be an old basement fault that was reactivated after deposition of the Gardiner Sandstone.

Diagenetic-hydrothermal models for the formation of unconformity-associated uranium deposits, developed by Hoeve and Sibbald (1978), Hoeve et al. (1980), Maas (1989), Wilde et al. (1989), Solomon and Groves (1994) and Ruzicka (1996), propose that the deposition of uranium minerals occurred during the latter stages of diagenesis, when the unconformity was covered by several kilometres of overburden. If age constraints set by Crispe and Vandenberg (2005) are accepted, the unconformity at the base of the Birrindudu Group in the

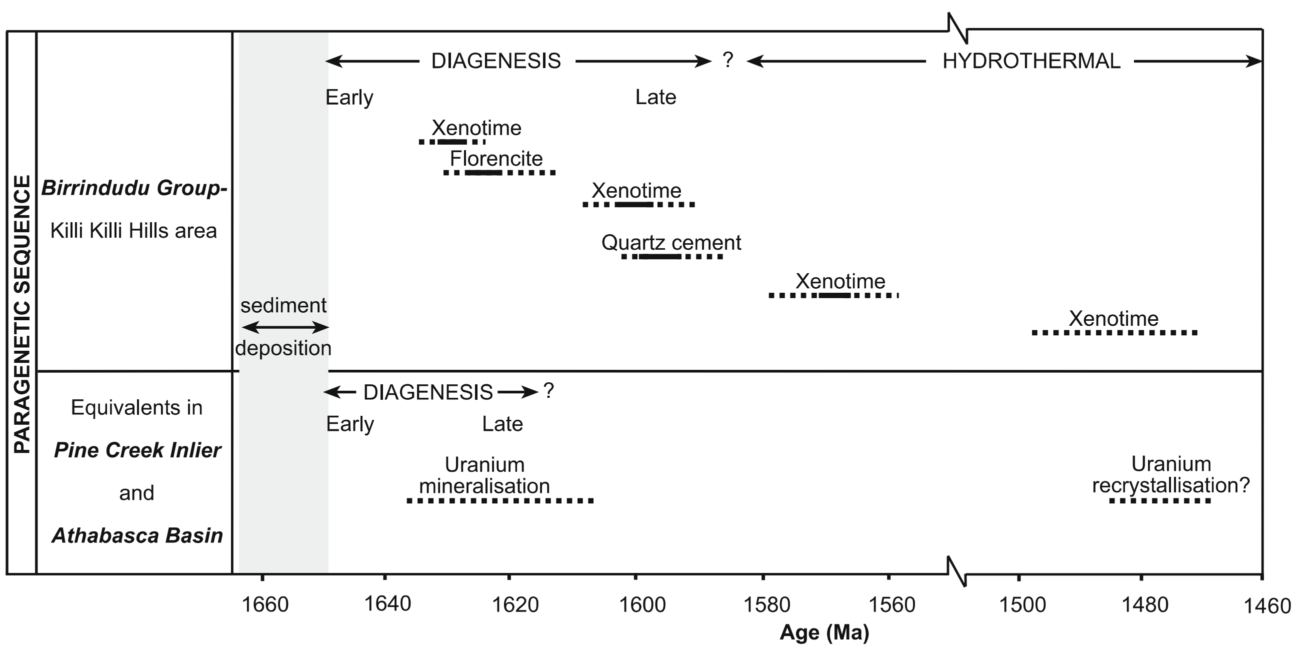

Fig. 5 Summary of the paragenetic sequence within the basal Gardiner Sandstone in the Killi Killi Hills. The approximate age of sediment deposition and primary uranium mineralisation (as well as a potential uranium recrystallisation event) in the Pine Creek Inlier (Page et al. 1980; Von Pechmann 1986; Maas 1989) and Athabasca Basin (Alexandre and Kyser 2003; Rainbird et al. 2005) is shown for reference. *Dashed lines* indicate uncertainty

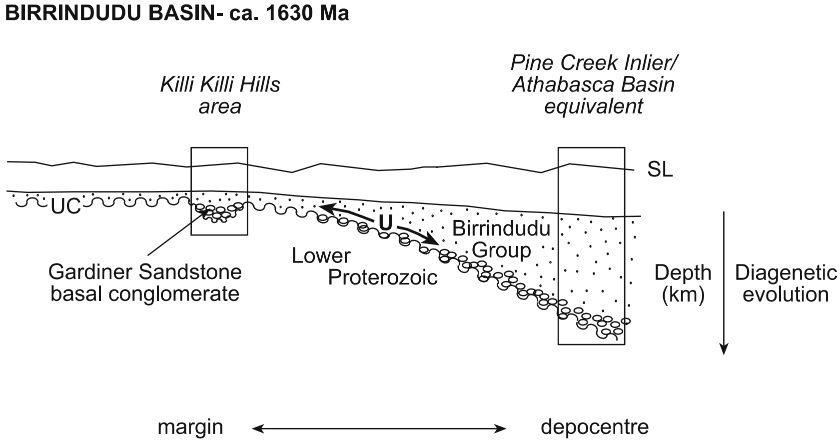

Fig. 6 Schematic diagram showing the inferred diachroneity of diagenesis developed across the Birrindudu Basin at the time of uranium mobilisation, assumed to be ca. 1,630 Ma. The inferred site of deposition for the Birrindudu Group in the Killi Killi Hills area is indicated relative to that inferred for unconformity-associated uranium deposits (*SL* sea level, *UC* unconformity)

Granites-Tanami Region must have been deeply buried at the time of deposition of the Limbunya Group (at ca. 1,635 Ma) in the Victoria River Region to the north. This would place the sediments that formed the Birrindudu Group in the Granites-Tanami Region in the latter stages of diagenesis during the ca. 1,630 Ma uranium mobilisation event. However, sediments at the unconformity in the Killi Killi Hills area at that time were not at such an evolved level of diagenesis as diagenetic quartz cementation had not yet occurred. The paragenetic sequence preserved in the Gardiner Sandstone at Killi Killi Hills is summarised and plotted with reference to the approximate age of primary uranium mineralisation and onset of burial of the unconformity in the Pine Creek Inlier (Gulson and Mizon 1980; Maas 1989; Page et al. 1980) and the Athabasca Basin (Alexandre and Kyser 2003; Rainbird et al. 2005) in Fig. 5. Unlike the proposed late diagenetic timing for the uranium deposits, the pore-filling uraniferous xenotime cements formed earlier, prior to late diagenetic quartz cementation.

Unconformity-associated uranium deposits record episodes of reworking and recrystallisation which had little effect on the main concentrations or economic viability of the deposits (c.f. Ruzicka 1996). Likewise, the later generations of equally uraniferous xenotime crystals show textural evidence for the reworking (i.e. dissolution and re-precipitation) of earlier-formed xenotime generations; for example, the textural variation across the xenotime crystal in Fig. 2b shows evidence for partial dissolution.

The source of uranium within the xenotime is likely to have been detrital, similar to that proposed for uranium deposits. The uranium is unlikely to have been sourced magmatically from nearby granitic intrusions, as the nearest known granitoids are 1,870–1,790 Ma in age (Smith 2001). Likewise, uranium is unlikely to have been sourced from the underlying Killi Killi Formation, as this Formation only contains background uranium values (Pritchard et al. 1960). It appears most likely that the uranium-rich intrusions of the ca. 1,815 Ma Coomarie Dome, to the east of the Killi Killi Hills, shed uranium-rich detrital sediments during uplift and weathering, and that these were incorporated, via palaeochannels (in the case of the Killi Killi Hills), into the younger, and in parts directly overlying, Gardiner Sandstone. The youngest detrital zircon population recorded in the Gardiner Sandstone from the Pargee Range is ca. 1,815 Ma (Crispe and Vandenberg 2005), the same age as the Coomarie Dome and the Nanny Goat Volcanics (Claoue-Long et al. 2001). The syenogranites composing the Dome contain accessory apatite (Crispe and Vandenberg 2005), which could have provided the phosphorous required for the concentration of xenotime in the detrital sediments in the Killi Killi Hills.

The cover sequence in the Killi Killi Hills area has a minimum depositional age of 1,632 ± 3 Ma, as provided by the earliest diagenetic xenotime generation in the Gardiner Sandstone. If the Limbunya Group does indeed overlie the Birrindudu Group, the depositional age of the Birrindudu Group is likely to be at least 20–30 m y older than this minimum age. This would make it similar to the age range given for the Katherine River Group in the South Alligator and Alligator uranium fields, and its equivalent, the Tolmer Group in the Rum Jungle Area, which form the cover sequences to the uranium deposits in those areas. For example, the Kombolgie Formation, at the base of the Katherine River Group, has a minimum age of 1,648 ± 29 Ma (Page et al. 1980), based on SHRIMP U–Pb zircon data from an interbedded volcanic member.

The age of the main uranium host rocks in the Athabasca Basin, the siliciclastic Athabasca Group, is not precisely known. The Wolverine Point Formation, towards the middle of the Group, contains a small population of ca. 1,650 Ma detrital zircons (Rainbird et al. 2005) and a reworked tuff layer containing primary zircon has a U–Pb age of 1,644 ± 13 Ma (Rainbird et al. 2005). The tuff age is considered to represent the age of deposition for the Wolverine Point Formation. Strat-abound phosphate (apatite and minor xenotime) cements, which are present at several stratigraphic levels of the Athabasca Group, particularly the Manitou Falls Formation and Wolverine Point Formation (lower to middle Athabasca Group), were studied by Rainbird et al. (2003). In the Wolverine Point Formation, pore-filling apatite, some of which is concentrated along the reworked tuff horizons, texturally post-dates smaller early-diagenetic xenotime overgrowths on detrital zircon grains and has patches that are uranium-rich, highly unusual for diagenetic apatite. SHRIMP U–Pb geochronology of diagenetic apatite is not normally achievable, but uraniferous apatite from the Manitou Falls and Wolverine Point Formations yields $^{207}Pb/^{206}Pb$ ages of 1,625 ± 17 Ma and 1,638 ± 12 Ma, respectively (Rainbird et al. 2003). The ages have overlapping analytical uncertainty and are interpreted to record the same fluid event. Apatite cementation therefore occurred shortly after deposition of the Wolverine Point Formation.

The age of uranium mineralisation, in the form of diagenetic uraniferous xenotime, in the Killi Killi Hills area is broadly coeval with that of primary uranium mineralisation in the Pine Creek Inlier (see Gulson and Mizon 1980; Page et al. 1980; Von Pechmann 1986; Maas 1989) and Athabasca Basin (see Alexandre and Kyser 2003). Thus, within the age uncertainties of available data, it appears likely that the sedimentation and primary mineralisation ages in the Athabasca Basin, Pine Creek Inlier and this study are all the same or similar.

Implications

It is proposed that the uraniferous xenotime layer in the Killi Kill Hills formed at a similar time and by similar processes to those for unconformity-associated uranium deposits, except at a shallower depth and with less fluid focus. One explanation is that the uraniferous xenotime-rich zones represent remote distal "low-grade" zones along strike from higher-grade unconformity-associated ores. This is allowed within available geochronological constraints, and is likely given the similarity in ages between xenotime formation and uranium mineralisation in the Pine Creek Inlier and Athabasca Basin.

The apparent anomaly between the diagenetic environment of the sediments in the Killi Killi Hills area at ca. 1,630 Ma, compared to that in unconformity-associated uranium deposits at the time of uranium mineralisation (see Fig. 6), could be explained if the Killi Killi Hills area was originally located in the margins of the Birrindudu Basin (Fig. 6). The uranium provinces, such as those in the Pine Creek Inlier (Fig. 1), are inferred to have been located within the deeper parts of their basins at the time of uranium mobilisation so as to match the temperature and pressure data obtained by Koul et al. (1988) and Wilde et al. (1989) from the deposits in the Alligator Uranium Field. The relative lack of sediment cover, as well as local structural simplicity, combined with high phosphorous in the environment, may explain the lack of concentration of uranium into ore-grade zones in the Killi Killi Hills area at ca. 1,630 Ma, seemingly a time of major uranium mobilisation in basins across northern Australia.

An alternative model is that the xenotime layer represents an early stage of uranium concentration prior to uraninite formation. In such a model, this xenotime could represent a source of uranium which, during the latter stages of diagenesis, was leached from the xenotime cements and either replaced by uraninite or mobilised to form higher-grade uranium deposits elsewhere. However, uranium mobility has not occurred in the Killi Killi Hills area as uranium appears to have been conserved during later fluid-flow events.

Uraninite U–Pb geochronology does not normally yield robust mineralisation ages, as uraninite suffers from Pb-loss, resulting in apparently younger ages. Xenotime, on the other hand, is an extremely robust mineral for geochronology which can provide relatively precise ages for low-grade uranium mineralisation and recrystallisation events. Thus, if the xenotime-enriched areas at Killi Killi Hills do represent remote distal parts of unconformity-associated uranium deposits, they provide a reliable way to isotopically date the deposit-forming processes (c.f. Fig. 6). Alternatively, if they are indeed simply earlier in the diagenetic sequence, they provide a maximum age constraint for, but one probably very close to, the age of the unconformity-associated deposits. Likewise, it is possible that the ca. 1,630 Ma stratabound apatite cements dated by Rainbird et al. (2003) in the Athabasca Basin record the same fluid migration episode that was responsible for primary uranium mineralisation in the Athabasca Basin.

Conclusions

The strong similarities in geological setting, presence of stratabound phosphate cements, age complexity of mineralisation, and process of formation between the stratabound uraniferous xenotime cements in the Killi Killi Hills area, and the unconformity-associated uranium deposits in the Pine Creek Inlier and Athabasca Basin (Hoeve and Sibbald 1978; Hoeve et al. 1980; Maas 1989; Wilde et al. 1989; Solomon and Groves 1994; and Ruzicka 1996) are unlikely to be fortuitous and implicate a genetic link.

The xenotime crystals in the Gardiner Sandstone, Killi Killi Hills, record a diagenetic formation age of 1,632 ± 3 Ma which is interpreted to represent the minimum depositional age of the basal Birrindudu Group. The xenotime-hosted uranium-enrichment is broadly coeval with uranium mineralisation in the deposits of the Pine Creek Inlier and the Athabasca Basin. However, the uraniferous xenotime is texturally earlier than the commonly proposed, late-diagenetic timing of uraninite in the unconformity-associated uranium deposits. This could be explained if the Killi Killi Hills area was in the marginal areas of the sedimentary basin with less sedimentary cover at the time of uranium mobilisation across north Australian basins. In the Killi Killi Hills area, xenotime either records the primary uranium mineralisation event, but within a remote distal setting, or is a precursor uranium-rich source for unconformity-associated uranium deposits which form during later diagenesis. If so, such uraniferous xenotime layers could define prospective source horizons for uranium ore deposits and provide regional markers in exploration.

Xenotime provides a more robust mineral for dating than uraninite, but has not been recorded from ore zones of unconformity-associated uranium deposits. A potentially productive approach would be to search for syn-ore xenotime in the lateral zones of the ore environments of unconformity-associated uranium deposits. If present, in situ U–Pb dating, combined with detailed petrography, could provide robust and precise ages and, together with the very distal diagenetic xenotime, place tight constraints on the timing of primary uranium mineralisation within the history of the basin.

Acknowledgements The authors wish to thank Geoscience Australia, especially Elizabeth Webber, Andrew Cross and David Huston, for access to samples and documentation. The authors are also indebted to Rob Rainbird, from the NRC Canada, for his advice on the Athabasca Basin uranium deposits and for the pre-print of his paper. Thanks are also extended to Brendan Griffin and the staff at the Centre for Microscopy and Microanalysis, University of Western Australia, and to Marion Marshall at Minsep Laboratories, for their individual expertise and technical assistance. This paper was considerably improved in response to comments by J. Claoue-Long and I. Williams. This work was supported by an Australian Research Council (ARC) grant to N.J. McNaughton and B. Rasmussen. Xenotime analyses were performed at the Western Australian SHRIMP II facilities operated by a WA university-government consortium with ARC support. This study is part of a PhD thesis by the first author which is currently being completed at the University of Western Australia.

References

Alexandre P, Kyser K (2003) Geochronology of the Paleoproterozoic basement-hosted unconformity-type uranium deposits in northern Saskatchewan, Canada (extended abstract). In: Cuney M (ed) Uranium geochemistry 2003: uranium deposits-natural analogs-environment. International Conference Proceedings, Nancy, France, pp 37–40

Blake DH, Hodgson IM, Smith PA (1972) Geology of the Birrindudu and Tanami 1:250 000 sheet areas, Northern Territory. Bureau of Mineral Resources, Report 174

Blake DH, Hodgson IM, Muhling PC (1973) Geology of the Granites and Precambrian parts of the Billiluna, Lucas and Stansmore 1:250 000 sheet areas, Northern Territory and Western Australia. Bureau of Mineral Resources, Record 1973/171

Blake DH, Hodgson IM, Muhling PC (1979) Geology of the Granites-Tanami Region. Bureau of Mineral Resources Bulletin 197:1–91

Casey JN, Wells AT (1964) The geology of the north-east Canning Basin, Western Australia. Bureau of Mineral Resources, Report 49, pp 1–62

Cathles LM, Smith AT (1983) Thermal constraints on the formation of Mississippi Valley-type lead-zinc deposits and their implications for episodic basin dewatering and deposit genesis. Econ Geol 78:983–1002

Claoue-Long J, Cross A, Smith J (2001) NTGS-AGSO Geochronology Project, Report 4. Professional Opinion Series. Australian Geological Survey Organisation, Report 2001/06

Clark AB, Blockley JG (1960) A report on a geological reconnaissance, Billiluna Area (authority to prospect 769, Northern Territory). Open File, New Consolidated Gold Fields (Australasia) Pty. Limited, pp 1–9

Crispe A, Vandenberg L (2005) Geology of the Tanami Region, Northern Territory. Northern Territory Geological Survey Bulletin

Cumming GL, Krstic D (1992) The age of unconformity-related uranium mineralisation in the Athabasca Basin, northern Saskatchewan. Can J Earth Sci 29:1623–1639

Dean AA (2001) Igneous rocks of the Tanami Region. Northern Territory Geological Survey Record 2001-003

Fletcher IR, Rasmussen B, McNaughton NJ (2000) SHRIMP U–Pb geochronology of authigenic xenotime and its potential for dating sedimentary basins. Aust J Earth Sci 47:845–859

Fletcher IR, McNaughton NJ, Aleinikoff JA, Rasmussen B, Kamo SL (2004) Improved calibration procedures and new standards for U–Pb and Th–Pb dating of Phanerozoic xenotime by ion microprobe. Chem Geol 209:295–314

Gulson BL, Mizon KJ (1980) Lead isotope studies at Jabiluka. In: Ferguson J, Goleby A (eds) Uranium in the Pine Creek Geosyncline. International Atomic Energy Agency, Vienna, pp 439–456

Hanley LM, Wingate MTD (2000) SHRIMP zircon age for an Early Cambrian dolerite dyke: an intrusive phase of the Antrim Plateau Volcanics of Northern Australia. Aust J Earth Sci 47/6:1029–1040

Hendrickx M, Slater K, Crispe A, Dean A, Vandenburg L, Smith J (2000) Palaeoproterozoic stratigraphy of the Tanami Region: regional correlations and relation to mineralisation-preliminary results. Northern Territory Geological Survey Record GS 2000-13, pp 1–66

Hills JH, Richards JR (1976) Pitchblendes and galena ages in the Alligator Rivers region, Northern Territory, Australia. Mineralium Deposita 11:133–154

Hoeve J, Sibbald TII (1978) On the genesis of the Rabbit Lake and other unconformity-type uranium deposits in northern Saskatchewan, Canada. Econ Geol 73:1450–1473

Hoeve J, Sibbald TII, Ramaekers P, Lewry JF (1980) Athabasca Basin unconformity-type uranium deposits: a special class of sandstone-type deposits? In: Ferguson J, Goleby A (eds) Uranium in the Pine Creek Geosyncline. International Atomic Energy Agency, Vienna, pp 575–594

Jagodzinski EA, Wyborn LAI, Heinrich CA (1992) A report on the potential of the Granites-Tanami Block for unconformity style Au-Pt-Pd ± U mineralisation. Australian Geological Survey Organisation Minerals and Land Use Program Professional Opinion 1992/4, pp 1–26

Johnston JD, Wall VJ (1984) Why unconformity-related U deposits are unconformity related. Geol Soc Aust Abst 12:617–629

Kositcin N, McNaughton NJ, Griffin BJ, Fletcher IR, Groves DI, Rasmussen B (2003) Textural and geochemical discrimination between xenotime of different origin in the Archean Witwatersrand Basin, South Africa. Geochim Cosmochim Acta 67:709–731

Kotzer TG, Kyser TK (1990) The use of stable and radiogenic isotopes in the identification of fluids and processes associated with unconformity-type uranium deposits. In: Beck LS, Sibbald TII (eds) Modern exploration techniques, vol 9. Saskatchewan Geological Society Special Publication, pp 115–131

Koul S, Wilde AR, Tickoo AW (1988) A thermal history of the Proterozoic East Alligator River terrain, Northern Territory, Australia: a fission track study. Tectonophysics 145:101–112

Ludwig KR, Grauch RI, Nutt CJ, Nash JT, Frishman D, Simmons KR (1987) Age of uranium mineralisation at Jabiluka and Ranger deposits, Northern Territory, Australia: New U/Pb isotope evidence. Econ Geol 82:857–874

Maas R (1989) Nd–Sr isotope constraints on the age and origin of unconformity-type uranium deposits in the Alligator Rivers uranium field, Northern Territory, Australia. Econ Geol 84:64–90

McNaughton NJ, Rasmussen B, Fletcher IR (1999) SHRIMP uranium-lead dating of diagenetic xenotime in siliciclastic sedimentary rocks. Science 285:78–80

Page RW, Compston W, Needham RS (1980) Geochronology and evolution of the late Archaean basement and Proterozoic rocks in the Alligator Rivers uranium field, Northern Territory, Australia. In: Ferguson J, Goleby A (eds) Uranium in the Pine Creek Geosyncline. Vienna, International Atomic Energy Agency, pp 36–68

Page R, Sun SS, Blake D (1995) Geochronology of an exposed late Archaean basement terrane in The Granite-Tanami region. AGSO Res Newslett 22:19–20

Pritchard CE, Dallwitz WB, Roberts WMB (1960) The Killi Killi uranium prospects, Western Australia. Bureau of Mineral Resources, Record 1960/140

Rainbird RH, Rayner N, Stern RA (2003) SHRIMP U/Pb geochronology of apatite cements and zircon-bearing tuff clasts in sandstones from the Athabasca Group, Athabasca Basin, northern Saskatchewan and Alberta. Saskatchewan Industry and Resources Open House, Conference Proceedings Abstract Volume, pp 6

Rainbird RH, Stern RA, Rayner N, Jefferson CW (2005) Age, provenance and regional correlation of the Athabasca Group constrained by igneous and detrital zircon geochronology. In: Jefferson CW, Delaney GD (eds) Athabasca Extech IV Multidisciplinary Study, Northern Saskatchewan and Alberta. Geological Association of Canada, Geological Survey Canada, Saskatchewan Geological Survey

Rasmussen B (1996) Early diagenetic REE-phosphate minerals (florencite, gorceixite, crandellite, and xenotime) in marine sandstones: a major sink for oceanic phosphorus. Am J Sci 296:601–632

Rasmussen B, Fletcher IR, Bengtson S, McNaughton NJ (2004) SHRIMP U–Pb dating of diagenetic xenotime in the Stirling Range Formation, Western Australia: 1.8 billion year minimum age for the Stirling biota. Precamb Res 133:329–337

Ruzicka V (1996) Unconformity-associated uranium. In: Eckstrand OR, Sinclair WD, Thorpe RI (eds) Geology of Canadian Mineral Deposit Types. Geological Survey of Canada, Geology of Canada, no. 8, pp 197–210

Sambridge MS, Compston W (1994) Mixture modelling of multicomponent data sets with application to ion-probe zircon ages. Earth Planet Sci Lett 128:373–390

Smith J (2000) NTGS-AGSO Geochronology Progress Report 3. Australian Geological Survey Organisation Professional Opinion 2000/27

Smith J (2001) Summary of Results, Joint NTGS-AGSO Age Determination Program 1999–2001. Northern Territory Geological Survey Record 2001–007, pp 1–52

Solomon M, Groves DI (1994) Proterozoic uranium-platinum group element-gold deposits of the Pine Creek Inlier and the Murphy Inlier. In: The Geology and Origin of Australia's Mineral Deposits, Oxford University Press, Oxford, pp 287–343

Traves DM, Casey JN, Wells AT (1956) The geology of the southwestern Canning Basin, Western Australia. Bureau of Mineral Resources, Report 29, pp 1–76

Vallini D, Rasmussen B, Krapez B, Fletcher IR, McNaughton NJ (2002) Obtaining diagenetic ages from metamorphosed sedimentary rocks: U/Pb dating of unusually coarse xenotime cement in phosphatic sandstone. Geology 30:1083–1086

Vallini D, Rasmussen B, Krapez B, Fletcher IR, McNaughton NJ (2005) Microtextures, geochemistry and geochronology of authigenic xenotime: constraining the cementation history of a Palaeoproterozoic metasedimentary sequence. Sedimentology 52:101–122

Vandenberg LC, Hendrickx MA, Crispe AJ (2001) Structural geology of the Tanami Region. Northern Territory Geological Survey Record, 2001-004

Von Pechmann E (1986) Mineralogy, age dating, and genesis of the Kylie and Spring Creek uranium prospects, Waterhouse Complex. In: Craig JR, Hagni RD, Kiels W, Lange IM, Petrovskaya NV, Shadlun TN, Udubasa G, Augustithis SS (eds) Mineral Paragenesis. Theophrastus Publications SA, Athens, pp 303–343

Wilde AR, Mernagh TP, Bloom MS, Hoffmann CF (1989) Fluid inclusion evidence on the origin of some Australian unconformity-related uranium deposits. Econ Geol 84:1627–1642